

14 percent of the thermal H will have the necessary velocity of 2.9 km sec⁻¹, and chemical reactions can produce additional energetic H atoms (19). Hydrogen atoms leaving Titan with a velocity of 1.9 km sec⁻¹ directed backward and forward along Titan's orbit would enter orbits taking them as close as 5.6 R_S and as far as 180 R_S from Saturn. The observed confinement of the H between 8 and 25 R_S can probably be explained by the fact that the lifetime of neutral hydrogen against ionization is ~ 10⁸ sec between 10 and 21 R_S but falls rapidly by a factor of 100 inside and outside this region (21).

This lifetime is a factor of 10 longer than earlier estimates (1). If we use the new lifetime, and include the new estimates of the H density and the size of the torus reported here, the H supply rate from Titan is reduced by a factor of 2 to 1 × 10²⁷ atoms per second. Titan model atmosphere calculations (24, 25) yield escape rates of this magnitude for both H and H₂, although Allen *et al.* (26) have obtained Titan loss rates for H and H₂ an order of magnitude higher. The long H lifetime means that collisions may be important in the torus. For a density of 20 cm⁻³, the mean time between collisions is ~ 10⁸ seconds, about the same as the H lifetime. It is possible that the H₂ density in the torus exceeds the H density (1), so that collisions would dominate the H distribution and treatment of individual particle orbits would not be useful. The appropriate formulation for a collision-dominated cloud (24) shows that its characteristic scale (to the 1/e density level) would be 8 R_S for a cloud temperature of 260 K.

B. R. SANDEL, D. E. SHEMANSKY
A. L. BROADFOOT, J. B. HOLBERG
G. R. SMITH

*Earth and Space Sciences Institute,
University of Southern California,
Tucson, Arizona 85713*

J. C. MCCONNELL

*York University,
Ontario, Canada M3J 1V3*

D. F. STROBEL

*Naval Research Laboratory,
Washington, D.C. 20375*

S. K. ATREYA, T. M. DONAHUE
*University of Michigan,
Ann Arbor 48109*

H. W. MOOS

*Johns Hopkins University,
Baltimore, Maryland 21218*

D. M. HUNTEN

*University of Arizona,
Tucson 85721*

R. B. POMPHELY, S. LINICK
*Jet Propulsion Laboratory,
Pasadena, California 91103*

References and Notes

1. A. L. Broadfoot *et al.*, *Science* **212**, 206 (1981).
2. The planet's brightness at He 584 Å is proportional to the flux in the solar 584-Å line, and the He 584-Å solar flux inferred from its correlation with the solar 10.7-cm flux is about the same at the two encounters. This implies a change in the atmosphere.
3. J. C. McConnell, B. R. Sandel, A. L. Broadfoot, *Planet. Space Sci.* **29**, 283 (1981).
4. The eddy diffusion coefficient *K* describes the effectiveness of vertical mixing of the atmosphere.
5. L. Wallace and D. M. Hunten, *Astrophys. J.* **182**, 1013 (1973).
6. Y. L. Yung and D. F. Strobel, *ibid.* **239**, 395 (1980).
7. J. C. McConnell *et al.*, in preparation.
8. A. L. Broadfoot *et al.*, *J. Geophys. Res.* **86**, 8259 (1981).
9. D. E. Shemansky *et al.*, in preparation.
10. J. M. Ajello, S. K. Srivastava, Y. L. Yung, G. R. Gladstone, in preparation.
11. D. E. Gerhart, *J. Chem. Phys.* **62**, 821 (1975).
12. B. R. Sandel and A. L. Broadfoot, *Nature (London)* **292**, 679 (1981).
13. M. L. Kaiser, M. D. Desch, A. Lecacheux, *ibid.*, p. 731.
14. L. W. Esposito, J. P. Dille, J. W. Fountain, *J. Geophys. Res.* **85**, 5948 (1980).
15. The absolute planetocentric ring radii quoted in this report are based on event times and a preliminary Voyager 2 trajectory from the Jet Propulsion Laboratory. At present the largest uncertainty in the absolute radii of features is due to uncertainty in the location of Saturn's north rotation pole. We have used a pole located at 1950.0 right ascension of 38.554° and a declination of 83.316°. Current uncertainties in these values allow for an error of up to 30 km in the location of features in the ring plane.
16. R. F. Donnelly and J. H. Pope, NOAA (Nat. Oceanic Atmos. Adm.) Tech. Rep. ERL 276-SEL 25 (1973).
17. B. Hapke, E. Wells, J. Wagner, W. Partlow, *Icarus*, in press.
18. J. W. Warwick *et al.*, *Science* **212**, 239 (1981).
19. D. F. Strobel and D. E. Shemansky, *J. Geophys. Res.*, in press.
20. G. R. Smith, D. F. Strobel, A. L. Broadfoot, B. R. Sandel, D. E. Shemansky, J. B. Holberg, *J. Geophys. Res.*, in press.
21. H. S. Bridge *et al.*, *Science* **215**, 563 (1982).
22. T. R. McDonough and N. M. Brice, *Icarus* **20**, 136 (1973).
23. A *g* value is defined as the scattering rate of photons in a solar line from a single atom. This rate varies inversely with the square of solar distance.
24. D. M. Hunten, in *Planetary Satellites*, J. A. Burns, Ed. (Univ. of Arizona Press, Tucson, 1977), p. 420.
25. D. F. Strobel, *Icarus* **21**, 466 (1974).
26. M. Allen, J. P. Pinto, Y. L. Yung, *Astrophys. J.* **242**, L125 (1980).
27. We thank the Voyager Project personnel at JPL for the enthusiastic efforts that have made this mission a success. We also thank the staff of the Earth and Space Sciences Institute, Tucson, for their untiring support. This work was supported by the Jet Propulsion Laboratory, California Institute of Technology, under NASA contract NAS 7-100. Additional support was provided by the Planetary Sciences Discipline of NASA's Office of Space Sciences.

10 November 1981

Radio Science with Voyager 2 at Saturn: Atmosphere and Ionosphere and the Masses of Mimas, Tethys, and Iapetus

Abstract. *Voyager 2 radio occultation measurements of Saturn's atmosphere probed to the 1.2-bar pressure level, where the temperature was 143 ± 6 K and the lapse rate apparently equaled the dry adiabatic value of 0.85 K per kilometer. The tropopause at both mid-latitude occultation locations (36.5°N and 31°S) was at a pressure level of about 70 millibars and a temperature of approximately 82 K. The stratospheric structures were very similar with the temperature rising to about 140 K at the 1-millibar pressure level. The peak electron concentrations sensed were 1.7 × 10⁴ and 0.64 × 10⁴ per cubic centimeter in the predawn (31°S) and late afternoon (36.5°N) locations. The topside plasma scale heights were about 1000 kilometers for the late afternoon profile, and 260 kilometers for the lower portions and 1100 kilometers for the upper portions of the topside predawn ionosphere. Radio measurements of the masses of Tethys and Iapetus yield (7.55 ± 0.90) × 10²⁰ and (18.8 ± 1.2) × 10²⁰ kilograms respectively; the Tethys-Mimas resonance theory then provides a derived mass for Mimas of (0.455 ± 0.054) × 10²⁰ kilograms. These values for Tethys and Mimas represent major increases from previously accepted ground-based values, and appear to reverse a suggested trend of increasing satellite density with orbital radius in the Saturnian system. Current results suggest the opposite trend, in which the intermediate-sized satellites of Saturn may represent several classes of objects that differ with respect to the relative amounts of water, ammonia, and methane ices incorporated at different temperatures during formation. The anomalously low density of Iapetus might then be explained as resulting from a large hydrocarbon content, and its unusually dark surface markings as another manifestation of this same material.*

Radio science observations at Saturn with Voyager 2 included (i) mid-latitude occultation studies in the northern and southern hemispheres, (ii) new, direct determinations of the masses of Tethys and Iapetus from radio tracking and an indirect determination of the mass of Mimas, and (iii) measurement of the near forward microwave scattering from ring C. Here we present results for the

atmosphere and ionosphere of Saturn and the masses of Mimas, Tethys, and Iapetus (1, 2), plus a discussion of the mean densities of the satellites. The emphasis on various topics in this report reflects only the current state of our work. Other important questions, such as the structure of the lower ionosphere and the figure of Saturn, must await complete reduction of the data and the

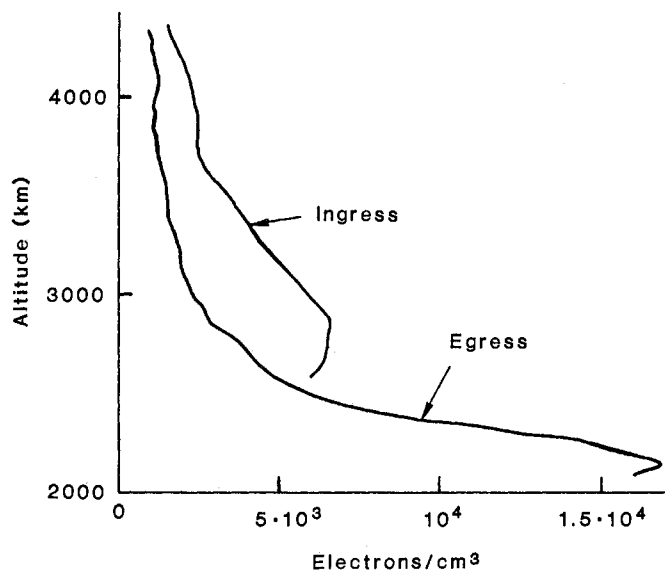
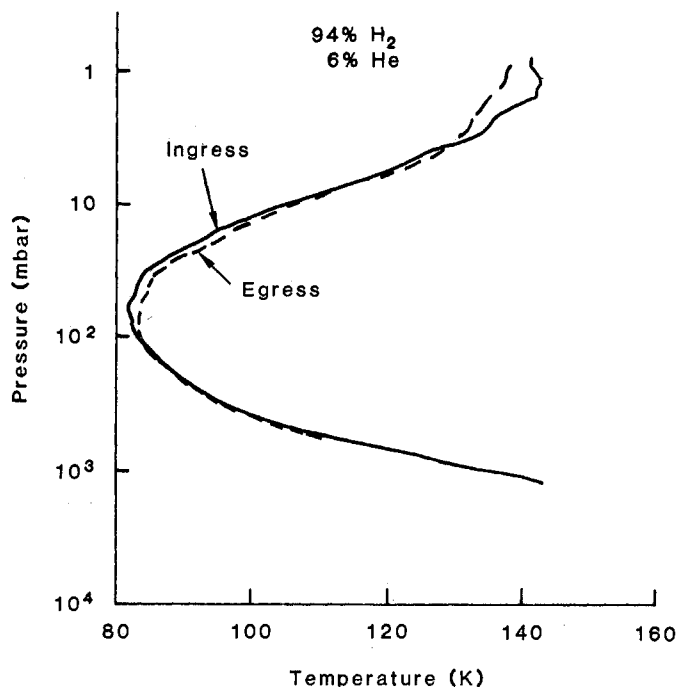


Fig. 1 (left). Atmospheric temperature-pressure profiles from the Voyager 2 mid-latitude occultations at Saturn, assuming an atmosphere of 94 percent H_2 and 6 percent He by volume. Fig. 2 (right). Concentration of electrons as a function of altitude above the

1-bar pressure level for the ionosphere of Saturn. The ingress was at $36.5^\circ N$ near the evening terminator, where the solar zenith angle was 87° . Egress was at $31^\circ S$ latitude under predawn conditions, where the zenith angle was 93° .

final refinements of the spacecraft trajectory. Experimental protocols and the pertinent spacecraft and mission characteristics have been described (3), as have other objectives of the radio science investigation (4, 5).

All observations reported here were carried out with the coherent dual-frequency radio system, which is also used for telemetry and navigation. The microwave frequencies employed are in an exact $11/3$ ratio, with wavelengths of 3.6 and 13 cm. The radio occultation signals were received at the 64-m-diameter NASA Deep Space Network tracking station at Ballima, New South Wales, Australia. For determination of the satellite masses we employed data from the worldwide NASA deep space stations.

Atmosphere and ionosphere of Saturn. The Voyager 2 trajectory, although constrained to carry the spacecraft toward Uranus, provided a nearly diametric Earth occultation geometry. Occultation immersion at Saturn was in the North Temperate Belt (6) at $36.5^\circ N$; emersion occurred at $31^\circ S$. The solar zenith angle for the immersion and emersion measurements were about 88° (late afternoon) and 94° (predawn) at the lowest altitudes probed for each of the two locations. With respect to the mean atmosphere observed by Voyager, $36.5^\circ N$ corresponds to a region of minimum atmospheric velocity with respect to the radio rotation rate, while $31^\circ S$ corresponds to a local eastward jet of about 100 m/sec with respect to the radio rotation (6).

Our results for the neutral atmosphere are presented in Fig. 1, where the derived temperature-pressure structure, assuming a gas mixture of 94 percent H_2 and 6 percent He (7) by volume, is shown for both locations. The data employed for Fig. 1 were measurements of the received signal frequency obtained in near real time with both the 3.6- and 13-cm wavelengths and automatic tracking receivers at the antenna site (8). During occultation entrance the 13-cm receivers followed the signal to the 1.2-bar level, where the atmospheric temperature was 143 ± 6 K. Translation of the ray in the horizontal direction (approximately north-south) was only about 0.4° of latitude (~ 400 km) over the entire range of the immersion curve. The receivers reacquired the signals during occultation emersion at the 600-mbar level and continued to track to and beyond the top of the neutral atmosphere. To the accuracy of the preliminary analysis, the temperature lapse rate appears to equal the adiabatic lapse rate of about 0.85 K km^{-1} in the lower part of the observed entry profile. The minimum tropopause temperature of 82 to 83 K occurs at a pressure of 60 to 75 mbar, and the stratospheric temperature at both locations rises to the vicinity of 140 K at the 1-mbar pressure level.

These results can be compared with those from Voyager 1 for $\sim 76^\circ S$ by shifting the published Voyager 1 curve 3.6 percent to the left and 6.6 percent up to compensate for the higher assumed fraction of He used in the reduction of

the Voyager 1 data (3). After this adjustment, there are some differences in the results that mainly appear in the approximately 5 K higher tropopause temperature obtained with Voyager 1 near the south pole. At present we have not evaluated the significance of this difference. We are cautious about its interpretation because the Voyager 1 ray path slipped a large distance horizontally (~ 8000 km) while the ray penetrated vertically only a relatively thin atmospheric shell (~ 200 km) (9). In view of the strong latitudinal temperature gradients reported by the Voyager IRIS investigation (7), the Voyager 1 immersion data could be affected by departure from hydrostatic equilibrium. We consider the Voyager 2 results more reliable than those of Voyager 1 on the basis of the improved experimental geometry for Voyager 2. When the possible uncertainties associated with the long sampling path of Voyager 1 are considered, the similarity of the three curves obtained thus far is remarkable, in marked contrast to large (~ 25 K) differences in stratospheric temperatures inferred over latitude ranges as small as 12° at Jupiter (10).

Figure 2 gives our results for the topside ionosphere at the two occultation points. These profiles were obtained by inversion of the differential dual-frequency observations at the 3.6- and 13-cm wavelengths. The peak concentration reached thus far with Voyager 2 was 1.7×10^4 e^- cm^{-3} , which was obtained about 2150 km above the 1-bar pressure level in the neutral atmosphere at the

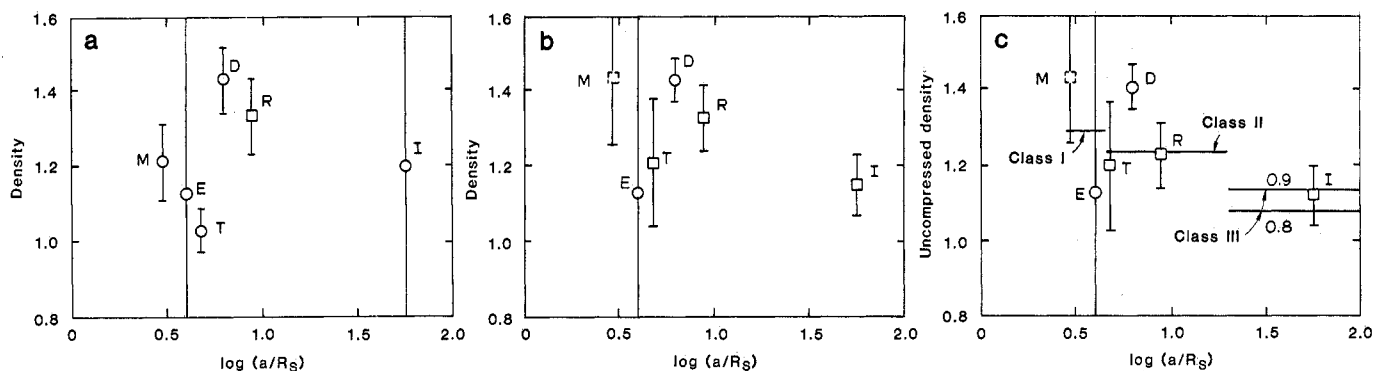


Fig. 3. Mean densities of the subject intermediate-sized satellites of Saturn as a function of their orbital radii. Squares represent values determined from Voyager measurements of both size and mass; circles include non-Voyager values, as described in the text. The dashed square represents an indirect but Voyager-derived determination of density. (a) Results as they appeared after Voyager 1 measurements. (b) Results after the Voyager 2 measurements. (c) Mean densities of (b) corrected to uncompressed densities for comparison with a model for the production of three classes of satellites, as described in the text.

31°S occultation emersion point. The late afternoon immersion profile is quite different, with what appears to be the peak of the main layer at a number density of $0.64 \times 10^4 \text{ e}^- \text{ cm}^{-3}$ and an altitude of about 2850 km. The altitude of the ionospheric peak measured by Voyager 1 at 73°S (near the evening terminator, where the solar zenith angle was 89°) lies between the two Voyager 2 values, and its peak density, at $2.4 \times 10^4 \text{ e}^- \text{ cm}^{-3}$, was larger than the two mid-latitude Voyager 2 results.

From about 2800 to 4000 km, the immersion profile exhibits a plasma scale height of about 1000 km, nearly twice the value (560 km) measured at the Voyager 1 entry location. The Voyager 2 egress profile shows a range of topside plasma scale heights varying from about 260 km just above the peak to about 1100 km in the height range 2500 to 3500 km. While model ionospheres have been investigated (11), there appears to be no ready explanation for the unexpectedly low concentrations of electrons at the ionospheric peaks, or for details of the observed ionospheric characteristics, such as the differences in peak altitudes, densities, and topside plasma scale heights for the various latitudes and times of day of the Saturn measurements.

While the given profiles are not expected to change, future work will result in the extension of both the atmospheric and ionospheric results to lower altitudes. It is possible—and seems likely based on the spectral characteristics of the signals—that additional, more complex ionospheric structures exist below the regions shown in Fig. 2.

Satellite masses and densities. The radio science experiment has yielded new values for the masses of five Saturnian satellites. Voyager 1 provided results for Titan and Rhea (3), and the Voyager 2 data constitute relatively di-

rect measurements of the masses of Tethys and Iapetus. Our new values for Tethys and Iapetus are $(7.55 \pm 0.90) \times 10^{20}$ and $(18.8 \pm 1.2) \times 10^{20}$ kg, respectively. The new mass for Tethys, in conjunction with the theory of the Tethys-Mimas resonance, provides a derived mass of Mimas of $(0.455 \pm 0.054) \times 10^{20}$ kg. For Mimas, and particularly for Tethys, the Voyager 2 values represent an increase of approximately 20 percent over the accepted values from ground-base observations, and lie well outside the published uncertainties in the earlier determinations (12).

The markedly increased values for the masses of Tethys and Mimas, as directly and indirectly derived from the Voyager 2 radio measurements, apparently reverse the trend for increasing density with respect to orbital radius inferred previously for the intermediate-sized satellites of Saturn. The current results suggest instead that density tends to decrease with orbital radius, in accordance with the general trend for the Jupiter system and for the solar system overall. Further, from an interpretation of the new results, we suggest that future measurements may show the mass of Dione to be 10 to 15 percent less than that derived from ground-based measurements to date. Such a change would represent a shift of about 4 standard deviations from the present value.

The densities of the satellites are of particular interest since they are fundamental to considerations of their present composition, which in turn depends on conditions under which they formed. The Voyager 1 radio measurements of Titan's mass and radius provided a value of about 1.89 g cm^{-3} , as discussed by Tyler *et al.* (3), and the refined equatorial radius of 2575 ± 2 km reported by Lindal (13) yields a mean density of $1.881 \pm 0.004 \text{ g cm}^{-3}$, assuming Titan to

be spherical. We consider here the densities of the smaller moons for which mass and size determinations have been made. Because its much greater mass and size may set Titan in a class by itself, we do not include it in discussing the comparative densities of the other satellites of Saturn. The masses are derived from both spacecraft radio and ground-based measurements, and the radii from Voyager optical measurements as interpreted by the imaging team (14). These intermediate-sized satellites, with radii ranging from about 200 to 750 km and orbital distances from about 3 to 60 Saturn radii (R_S), may constitute a set of comparable objects whose densities can provide clues to the conditions that existed during the formation of the Saturn system and, by extension, of the solar system as a whole. This seems particularly relevant in view of the differences between previously accepted interpretations of satellite densities as a function of distance from Saturn and the pattern that obtains elsewhere in the solar system.

Figure 3a shows the mean densities of the subject satellites plotted as a function of the logarithm of their orbital distance, as derived after Voyager 1 but before the Voyager 2 measurements (3, 6). All radii are from Voyager 1, Rhea's mass is also a Voyager 1 radio measurement, and the mass of Iapetus is from the Pioneer 11 radio experiment (15). The masses of Mimas, Enceladus, Tethys, and Dione were derived by Kozai (12, 16) from long-term ground-based measurements of their orbits and considerations of the Mimas-Tethys and Enceladus-Dione orbital resonances. Smith *et al.* (6) offered possible explanations for the apparently greater densities of the more distant Dione and Rhea as compared with the nearer Mimas and Tethys, and for the apparently random deviations from a general trend of increasing density with

Table 1. Mass, size, and density of the intermediate-sized satellites of Saturn.

Satellite	Mean radius (km)	Mass ($\times 10^{20}$ kg)	Mean density (g cm^{-3})	Approximate uncompressed density (g cm^{-3})	Assumed solar class and its uncompressed density (g cm^{-3})
Mimas	196 ± 3	0.455 ± 0.054	1.44 ± 0.18	1.44 ± 0.18	I, 1.29
Enceladus	250 ± 10	0.74 ± 0.36	1.13 ± 0.55	1.13 ± 0.55	I, 1.29
Tethys	530 ± 10	7.55 ± 0.90	1.21 ± 0.17	1.20 ± 0.17	II, 1.24
Dione	560 ± 5	10.52 ± 0.33	1.43 ± 0.06	1.41 ± 0.06	II, 1.24
Rhea	765 ± 5	24.9 ± 1.5	1.33 ± 0.09	1.23 ± 0.09	II, 1.24
Iapetus	730 ± 10	18.8 ± 1.2	1.15 ± 0.08	1.12 ± 0.08	III, 1.09 to 1.14

orbital radius from Mimas to Titan. These explanations involve mechanisms by which the moons are made up of various fractions of rock and water ice that differ from their relative abundance in a primordial planetary nebula, through both selective and random dynamic processes during satellite formation. An alternative hypothesis maintains the concept that the solar composition of rock and other condensables remains controlling in each case. In this hypothesis, variation in the density is primarily a result of the general decrease in temperature with the orbital radius of formation, so that different condensables form ices at different radii (17). During formation the satellites collect solids—but not gases—from the ambient material and hence have different compositions depending on which material is solid at a given temperature. The apparent low density of Tethys compared with its neighbors was clearly inconsistent with this model; as a result, Prentice (17) suggested that the mass of Tethys might be 20 to 25 percent larger than the ground-based value of $(6.22 \pm 0.13) \times 10^{20}$ kg. This prediction represented a potential change of 10 to 12 standard deviations and was considered highly unlikely by many workers.

Table 1 and Fig. 3b present the post-Voyager 2 situation for the masses, radii, and mean densities of the six satellites. The Voyager 2 measurement of the Tethys mass of $(7.55 \pm 0.90) \times 10^{20}$ kg is 21.4 percent higher and 10 standard deviations from the value based on the Mimas-Tethys resonance (12, 16).

Since the ground-based value is only about 1.5 Voyager standard deviations from the Voyager result, the numbers suggest that it is the Voyager mean that is in error. However, we argue against such a conclusion on several grounds. First, while it is preliminary and more analysis is needed, the Voyager determination is a relatively direct measure of

the mass, involving radio measurements of the spacecraft trajectory in the vicinity of Tethys. By contrast, the long-term ground-based observations require detailed interpretive study and are based on a limited model of the system, as discussed below. Second, while the published uncertainties correctly reflect the errors assigned by the various ground-based observers, when used in a formal way in the libration theory, they may be unrealistically small since the theory may have failed to include significant long-term effects.

The ratio of the mass of Mimas to the mass of Tethys is determined from several decades of ground-based data on the libration in orbital longitudes for the two satellites, a libration driven by the resonance lock between them (18). We believe this ratio is less sensitive to limitations in the libration theory than are the individual masses. Thus we use this ratio to derive a new mass and hence density for Mimas based on the Voyager 2 determination of the mass of Tethys; these results are also given in Table 1 and Fig. 3b.

However, it is clear that much more work is needed on all fronts of this problem. When we use the Voyager 2 value for the Tethys mass to compute a mass for Mimas from the observed mass ratio, and then use both masses to compute a theoretical libration period, we obtain a value of 65.1 years, not the observed period of 71.1 years. We suggest that this discrepancy may be caused by a failure of the existing libration theory to predict the correct period. We have ruled out the possibilities that the observed period could be wrong or that an error in the mass ratio could be responsible for the discrepancy. Our independent analysis of the published libration data (12) yields a mass ratio of 0.06031 with a formal uncertainty of ± 0.00031 and an estimated realistic error of ± 0.00070 ; our libration period is

71.05 years with a formal error of ± 0.39 year and a realistic error of ± 0.78 year. These values differ insignificantly from those given by Kozai (0.06019 ± 0.00036 and 71.12 ± 0.22 years, respectively), except that we have been more conservative in estimating the error. Even so, our realistic error in the period implies that the theoretical period is about 8 standard deviations lower than the observed period.

The simplified dynamical model used for the libration theory may be a source of this problem. This model treats Saturn, Mimas, and Tethys as point masses and assumes that there are no other significant dynamical contributions to the libration. However, other effects may be important, even including the effects of previously unknown satellites. Work on this problem will continue, but we believe that at this stage the Voyager measurement of the Tethys mass, plus the mass ratio from ground-based data and the libration theory, yield the current best estimates of the masses of Tethys and Mimas.

Referring again to Table 1 and Fig. 3b, the uncertainty in the Iapetus density has been greatly reduced by the Voyager 2 determination of mass. Iapetus apparently has the lowest density of the satellites for which both mass and radius have been determined by, or inferred from, Voyager measurements. (The density of Enceladus remains too uncertain to be significant in the following discussion. However, further work involving a combination of Voyager and Pioneer 11 data should yield an improved value for Enceladus as well.)

There now appears to be a general trend of decreasing density with increasing orbital radius for the comparably sized icy satellites represented in Fig. 3b. This trend becomes more apparent if the observed mean densities are corrected to the density of the uncompressed material. However, there is an inherent conflict in computing such a correction because the degree of correction depends on the material involved, while the motive for obtaining the uncompressed densities is to help determine the possible chemical composition. Fortunately, in this case we are dealing with small bodies so that the corrections are not very large, and the final results for uncompressed densities are not likely to be appreciably affected by a particular choice of model composition.

An example of such a corrected result is summarized in the last two columns of Table 1 and in Fig. 3c. The particular model for the tabulated and pictured results is due to Prentice (19), who com-

puted the effects of compression for satellites that formed by thermochemical equilibrium condensation (20) from a solar mix of anhydrous rock, H₂O, NH₃, and CH₄. That is, the relative amount of each substance potentially available for incorporation in a given satellite is determined by the relative abundance of the corresponding elements observed in the sun (21). It is assumed that material is collected into the solid body only when the water, ammonia, or methane is frozen, so that the resultant mix is a function only of temperature at formation. Three such solar-mix classes, which correspond to formation in different temperature regimes, would then result: class I with 38 percent (by mass) rock and 62 percent H₂O ice; class II with 35 percent rock, 57 percent H₂O ice, and 8 percent NH₃ ice; and class III with 26 percent rock, 41 percent H₂O ice, 6 percent NH₃ ice, and 27 percent stable dense hydrocarbons, which are assumed to have been formed internally from the original store of methane (19). In class III, since pure CH₄ ice is now thermodynamically unstable at Saturn's distance from the sun (22), it is assumed that the carbon from the original methane remains at its relative solar abundance in these objects as denser and more stable hydrocarbons, such as heavily branched paraffins and aromatic ring structures (19).

The demarcation temperatures or orbital radii for these classes are also model-dependent. From the work of Prentice (17), class I objects would form between about 3 and 5 R_S , class II between 5 and 19 R_S , and class III beyond 19 R_S , where the temperature is first estimated to fall below the freezing point of methane. From this model, Mimas and Enceladus should be class I objects with an uncompressed density of 1.29 g cm⁻³ and Tethys, Dione, and Rhea should be class II with an uncompressed density of 1.24 g cm⁻³. The density of class III objects, where Iapetus would be the example, depends on the hydrocarbon density, which is taken to be between 0.8 and 0.9 g cm⁻³. This yields an uncompressed value between 1.09 and 1.14 g cm⁻³, as given in Table 1 and Fig. 3c.

The Voyager results are consistent with this picture, and in the cases of Tethys, Rhea, and Iapetus the correspondence appears remarkable. The fundamental point is that the uncompressed densities of these intermediate-sized icy satellites may depend on orbital radius alone, without the need for assumptions concerning sorting of nebular material before or during satellite formation. Our use of the example from Prentice (17)

does not depend on other aspects of his theory. The problem is complex, and fundamentally different theories may be equally successful in explaining these Voyager results. Nevertheless, the correspondences thus far lead us to consider that Dione might have a mass some 10 to 15 percent less than the presently accepted value mentioned above. This would bring it into conformity with the interpretation discussed above.

The mass of Dione was determined from the forced eccentricity in the orbit of Enceladus with a magnitude of about 0.0045 (23). In the absence of a commensurability, the natural eccentricity of Enceladus would be about 10⁻⁴ while the eccentricity of the orbit of Dione is about 0.002, with a negligible contribution from the forcing terms. Because of these small eccentricities, the Enceladus-Dione resonance presents one of the most difficult theoretical problems of the Saturn satellite system. We suggest that, as may have been the case for Tethys, the published uncertainty in the mass of Dione, based on ground-based observations, may not be realistic. Thus the change required to make Dione a class II object may not be as unlikely as published values imply.

Finally, a comment on the apparent low density of Iapetus. If Iapetus is indeed a class III object whose mass is on the order of one-quarter hydrocarbons, then it is unique compared with the planets and moons of the inner solar system and the other measured satellites of Jupiter and Saturn. The surface of Iapetus is unique in the large albedo contrast between leading and trailing hemispheres. We note the obvious possibility of a connection between the hypothesized large carbon content of Iapetus and the existence of dark surface material with an albedo consistent with that of carbonaceous chondrites (6), which in turn consist of up to 5 percent by mass of the type of complex hydrocarbons discussed above.

G. L. TYLER

V. R. ESHLEMAN

Center for Radar Astronomy,
Stanford University,
Stanford, California 94305

J. D. ANDERSON

G. S. LEVY

G. F. LINDAL

G. E. WOOD

Jet Propulsion Laboratory,
California Institute of Technology,
Pasadena 91109

T. A. CROFT

Radio Physics Laboratory,
SRI International,
Menlo Park, California 94025

References and Notes

1. We report occultation results based on "closed-loop" tracking (2) of the 13-cm signals. Occultation data were also obtained at 3.6 cm, but to a lesser depth in the atmosphere because of the extra loss induced at the shorter wavelength by microwave absorbers, probably mostly ammonia vapor. Results for the masses of Tethys and Iapetus are based on the use of the Voyager Deep Space Network Doppler tracking system. The observations of oblique scatter from ring C, which were designed to determine the centimeter-sized component of the particle size distribution, were an additional major objective of the radio experiment. The latter observations were recorded at the tracking station in Australia and then shipped to JPL for validation and delivery to the radio science team. The ring C data have not yet been analyzed. For the results of the radio science investigation by Voyager 1 at Saturn, see (3).
2. The radio system parameters are given in (4). For a general discussion of the radio system including telemetry, see R. E. Edleson, B. D. Madsen, E. K. Davis, G. W. Garrison, *Science* **204**, 913 (1979).
3. G. L. Tyler, V. R. Eshleman, J. D. Anderson, G. S. Levy, G. F. Lindal, G. E. Wood, T. A. Croft, *ibid.* **212**, 201 (1981).
4. V. R. Eshleman, G. L. Tyler, J. D. Anderson, G. F. Jeldbo, G. S. Levy, G. E. Wood, T. A. Croft, *Space Sci. Rev.* **21**, 207 (1977).
5. Other Voyager 2 objectives included measurements of the gravitational red shift of the spacecraft oscillator associated with the Saturnian potential well and studies of turbulence in the atmosphere and ionosphere of Saturn.
6. B. A. Smith *et al.*, *Science* **212**, 163 (1981).
7. R. Hanel *et al.*, *ibid.*, p. 192.
8. The results given here are based on data from the automatic phase-locked-loop tracking receiver located at the antenna site. For occultation immersion this system provides values of frequency continuously until the combination of decreasing signal strength, increasing signal dynamics, and errors in the predicted average signal frequency preclude continued reception. During occultation emersion the signal increases in strength but cannot be reliably detected and tracked until it is well above the point at which the immersion signal is lost. Consequently, preliminary results from occultation immersion are obtained to a greater depth in the atmosphere than those from emersion. Improved results will be obtained from the primary data that consist of a set of high-speed digital samples of the received signals, as yet undetected. These samples can be processed to yield both signal frequency and amplitude from greater depths in the atmosphere than is possible with the phase-locked system. Also see reference 4 in (3).
9. The grazing nature of the Voyager 1 occultation immersion resulted in considerable horizontal translation of the occultation ray through the atmosphere, with measurements extending from about 73°S at the lowest pressures sensed to about 79.5°S at the highest pressures sensed. This corresponds to a distance of approximately 8000 km perpendicular to the radio ray, while the vertical penetration is only 200 km. Inversion of the data relies on the assumption of hydrostatic equilibrium and uniformity of the temperature-pressure field over the region sampled. It is possible that there are systematic errors in the Voyager 1 profiles that result from violation of the assumed conditions. Further work is required to understand this problem better as specifically related to the Voyager 1 Saturn case.
10. G. F. Lindal *et al.*, *J. Geophys. Res.* **86**, 8721 (1981). The large temperature differences inferred for Jupiter were obtained under the assumption that the pressure profiles are the same in each of the several locations. The actual differences in the atmosphere could be a combination of local horizontal gradients in temperature and pressure.
11. M. B. McElroy, *Space Sci. Rev.* **14**, 460 (1973); S. K. Atreya and T. M. Donahue, *Icarus* **24**, 358 (1975); *ibid.* **25**, 335 (1975); S. K. Atreya and J. H. Waite, Jr., *Nature (London)* **292**, 682 (1981); J. H. Waite, Jr., thesis, University of Michigan (1981); M. Shimizu, *Moon Planets* **22**, 521 (1980).
12. The masses were determined by G. Struve [Veroff., Univ. Sternwarte, Berlin-Babelsberg, **4**, (1930)] with data from 1789 to 1927 and were discussed further by H. Jeffries [*Mon. Not. R. Astron. Soc.* **113**, 81 (1953)], who gave $(6.69 \pm 0.20) \times 10^{-8}$ and $(1.141 \pm 0.030) \times 10^{-6}$ for Mimas and Tethys, respectively, in units of the mass of Saturn. The most thorough discussion of the data has been given by Y. Kozai

- [*Ann. Tokyo Astron. Obs.* 5, 73 (1957)], who included more recent observations from 1927 and 1928 as well as data from the U.S. Naval Observatory between 1938 and 1947. He gives $(6.59 \pm 0.15) \times 10^{-8}$ and $(1.095 \pm 0.022) \times 10^{-6}$, respectively, where we have converted his probable errors to standard errors. For comparison with the mass, we use 5.684×10^{26} kg for Saturn.
13. G. F. Lindal, *Bull. Am. Astron. Soc.* 13, 700 (1981).
 14. Values of radii from the Voyager imaging team are as given in B. A. Smith *et al.*, *Science* 215, 504 (1982).
 15. G. W. Null, *Astron. J.* 81, 1153 (1976).
 16. Y. Kozai, *Publ. Astron. Soc. Jpn.* 28, 675 (1976).
 17. A. J. R. Prentice, *J. Astron. Soc. Victoria* 28, 47 (1981); *Bull. Am. Astron. Soc.* 13, 743 (1981); in *The Origin of the Solar System*, S. F. Dermott, Ed. (Wiley, London, 1978), pp. 111–162; _____ and D. ter Haar, *Nature (London)* 280, 300 (1979).
 18. On the average, the orbital motions of Mimas and Tethys are in a 4:2 commensurability ratio with respect to a uniformly rotating axis midway between their ascending nodes on the equator of Saturn. The theory of the forced libration about this resonance state was outlined by F. Tisserand [*Theorie de Mécanique Céleste* 4, 98 (1896)] and is discussed in more modern terms by L. Blitzer and J. D. Anderson (*Celest. Mech.*, in press). General reviews of orbit-orbit resonances in the solar system have been given by S. J. Peale [*Annu. Rev. Astron. Astrophys.* 14, 215 (1976)] and R. Greenberg [in *Planetary Satellites*, J. A. Burns, Ed. (Univ. of Arizona Press, Tucson 1977); *Vistas Astron.* 21, 209 (1977)].
 19. A. J. R. Prentice, private communication. A simplified numerical code was used to determine the effects of compression by assuming the satellites to be chemically undifferentiated and using the data of M. J. Lupo and J. S. Lewis [*Icarus* 40, 157 (1979)] for the compressibility of rock and ices. Water, ammonia, and methane ices were considered. A methane clathrate was also included in a model but was found not to define a distinctive class by density because of its low abundance.
 20. J. S. Lewis, *Icarus* 16, 241 (1972); *Science* 186, 440 (1974).
 21. J. E. Ross and L. H. Aller, *Science* 191, 1223 (1976).
 22. L. A. Lebofsky, *Icarus* 25, 205 (1975).
 23. Y. Kozai (16) determined the mass of Dione as $(1.85 \pm 0.04) \times 10^{-6}$ times the mass of Saturn by using the theory of M. Rapaport [*Astron. Astrophys.* 22, 179 (1973)] for the forced eccentricity.
 24. We thank the members of the Voyager Project operations team and the Deep Space Network for their support in the acquisition of the radio science data. We thank the Voyager navigation team for their help in preparing data files for the celestial mechanics phase of the investigation, for making their software available to us, and for giving us the benefit of their experience in fitting orbits to radio and optical navigation data. We particularly acknowledge the direct involvement of J. K. Campbell in the determination of masses for Tethys and Iapetus. We thank the Voyager imaging team for prepublication values of radii. We also thank A. J. R. Prentice for numerous discussions and assistance in calculations, plus prepublication results on model satellite densities. We especially thank B. J. Buckles, P. E. Doms, D. F. Finnerty, and D. P. Holmes for their help in the implementation and execution of these experiments, and H. B. Hotz and D. N. Sweetnam for their help in the occultation profile reduction. This work was supported by the National Aeronautics and Space Administration.

10 November 1981; revised 23 November 1981

Magnetic Field Studies by Voyager 2: Preliminary

Results at Saturn

Abstract. *Further studies of the Saturnian magnetosphere and planetary magnetic field by Voyager 2 have substantiated the earlier results derived from Voyager 1 observations in 1980. The magnetic field is primarily that of a centered dipole (moment = 0.21 gauss- R_S^3 ; where one Saturn radius, R_S , is 60,330 kilometers) tilted approximately 0.8° from the rotation axis. Near closest approach to Saturn, Voyager 2 traversed a kronographic longitude and latitude range that was complementary to that of Voyager 1. Somewhat surprisingly, no evidence was found in the data or the analysis for any large-scale magnetic anomaly in the northern hemisphere which could be associated with the periodic modulation of Saturnian kilometric radiation radio emissions. Voyager 2 crossed the magnetopause of a relatively compressed Saturnian magnetosphere at $18.5 R_S$ while inbound near the noon meridian. Outbound, near the dawn meridian, the magnetosphere had expanded considerably and the magnetopause boundary was not observed until the spacecraft reached 48.4 to $50.9 R_S$ and possibly beyond. Throughout the outbound magnetosphere passage, a period of 46 hours (4.5 Saturn rotations), the field was relatively steady and smooth showing no evidence for any azimuthal asymmetry or magnetic anomaly in the planetary field. We are thus left with a rather enigmatic situation to understand the basic source of Saturnian kilometric radiation modulation, other than the small dipole tilt.*

In this report we present results of a study of the magnetosphere and planetary magnetic field of Saturn as observed by Voyager 2. The magnetometers (1) operated normally throughout the encounter. The instrumentation of the Voyager 2 magnetic field experiment is identical to that on Voyager 1 (2) with the instrument automatically changing ranges as required by the measured field. The minimum quantization step size

of ± 0.0044 nanotesla (nT) in the lowest range of ± 8.8 nT full scale increased to ± 0.51 nT in the ± 2100 nT range near closest approach. As before (2), vector measurements at 60-msec intervals were averaged over 1.92, 9.6, and 48 seconds, 16 minutes, and 1 hour.

The maximum measured field intensity of 1187 nT was observed at a kronographic latitude of 17.3°N and longitude (Saturn longitude system, SLS) (3) of

322.3° , just before periapsis at $2.69 R_S$ ($R_S = 60,330$ km). This value was only a few nanoteslas larger than expected, based on a Voyager 1-derived model (2) magnetosphere, which had a centered dipole tilted 0.7° with magnetic moment 0.21 gauss- R_S^3 and an azimuthal equatorial ring current (4) of 7×10^6 A to represent the magnetic field for $R < 15 R_S$. The spacecraft crossed the equatorial plane only once, at $2.87 R_S$ just after closest approach. There were no special close encounters with any of the Saturnian satellites, such as were accomplished by Voyager 1 at Titan (2, 5), at least from the viewpoint of being within five or fewer satellite diameters.

The main objective for the magnetometer experiment was to determine the location and characteristics of the presumed northern hemisphere magnetic anomaly responsible for the periodic modulation of the Saturnian kilometric radiation (SKR) radio emissions (6). Another objective was to compare the magnetic field characteristics of the Saturnian magnetosphere with those observed by Voyager 1 and Pioneer 11.

Bow shock, magnetopause, and magnetosheath. Voyager 2 observed multiple bow shock and magnetopause (MP) crossings during its inbound and outbound trajectory. Figure 1 (right side) shows the trajectory of Voyager 2 in cylindrical coordinates. The axis of symmetry of the system is along the planet-sun line. A filled dot on the trajectory denotes start of a day (for example, 236 is 24 August 1981). For comparison, the Voyager 1 trajectory is shown (left side), also in cylindrical coordinates. The Voyager 1 model bow shock and MP boundaries (2) are also displayed. Table 1 gives a preliminary listing of bow shock and MP boundary crossing times and planetocentric radial distances, based on the Voyager 2 magnetometer data. There were multiple crossings of both boundaries: five inbound bow shocks, one inbound MP, at least five well-defined outbound MP's, and seven outbound bow shocks. The average inbound and outbound bow shock crossing positions are shown by line segments intersecting the Voyager 2 trajectory on days 236 and 242, respectively.

The MP of all known magnetospheres is most commonly observed to be a tangential magnetohydrodynamic discontinuity. To accurately estimate the direction normal to that boundary for the MP crossings in Table 1, we used a magnetic field variance method (7) well suited for analyzing tangential discontinuities. The analysis to determine the inbound normal yielded an estimate of